MRS Advances © 2018 Materials Research Society
DOI: 10.1557/adv.2018.278

Human Stem Cell Derived Osteocytes in Bone-on-Chip

E. Budyn[1,3], N. Gaci[1], S. Sanders[1], M. Bensidhoum[2], E. Schmidt[3], B. Cinquin[4], P. Tauc[4] and H. Petite[2]

[1] *LMT Laboratory CNRS UMR8535, ENS Cachan, Universite Paris-Saclay, 61 Avenue du Pres. Wilson, 94235 Cachan cedex, France*

[2] *B2OA Laboratory CNRS UMR7052, Universite Paris Diderot, 10 Avenue de Verdun, 75010 Paris, France*

[3] *Department of Mechanical Engineering, University of Illinois at Chicago, 842 W. Taylor St., Chicago, IL 60607, U.S.A.*

[4] *LBPA Laboratory CNRS UMR8113, ENS Cachan, Universite Paris-Saclay, 61 Avenue du Pres. Wilson, 94235 Cachan cedex, France*

ABSTRACT

Human mesenchymal stem cells were reseeded in decellularized human bone subject to a controlled mechanical loading to create a bone-on-chip that was cultured for over 26 months. The cell morphology and their secretome were characterized using immunohistochemistry and in situ immunofluorescence under confocal microscopy. The presence of stem cell derived osteocytes was confirmed at 547 days. Different cell populations were identified. Some cells were connected by long processes and formed a network. Comparison of the MSCs in vitro reorganization and calcium response to in situ mechanical stimulation were compared to MLOY4 cells reseeded on human bone. The bone-on-chip produced an ECM of which the strength was nearly a quarter of native bone after 109 days and that contained calcium minerals at 39 days and type I collagen at 256 days. The cytoplasmic calcium concentration variations seemed to adapt to the expected in vivo mechanical load at the successive stages of cell differentiation in agreement with studies using fluid shear flow stimulation. Some degree of bone-like formation over a long period of time with the formation of a newly formed matrix was observed.

INTRODUCTION

Large bone defects cannot repair. Such pathologies carry $10 billion financial burden on the U.S. healthcare system. Successful techniques promoting good quality tissue regeneration is complex and requires the addition of functional materials. Bone self-healing repair called remodeling is orchestrated by osteocytes upon the detection of microdamage [1–5]. Osteocytes derive from mesenchymal stem cells in the bone marrow and are at the center [6] of bone homeostasis and coordinate the interactions between the osteoclasts responsible for bone resorption and MSCs that will differentiate into osteoprogenitors and osteoblasts responsible for new bone formation in the remodeling process. Osteoblasts can then differentiate in osteocytes or bone lining cells [7,8] that cover non-remodeling endosteal bone surfaces and are also recruited during the activation phase of remodeling to seal the site of bone formation by osteoblasts, modulate the

osteoclastic resorption and further differentiate into osteoblasts [9]. The osteoblasts remain trapped in mineralizing osteoid and further differentiate into osteocytes. Osteocytes are long term living cells [10] that are responsible for bone mineralization and characterized and are mechano-sensitive being attached to the mineralized extra cellular matrix (ECM) by a pericellular matrix (PCM) rich in integrins [11,12] along their numerous processes. The load bearer layer of long bone is called Haversian bone in which osteons are lamellar tubular structures created from osteoclastic resorption that are filled by successive fibrous lamellae laid by osteoblasts after the recruitment of MSCs and bone lining cells. However many questions remain on why osteoblasts would produce a certain type of bone structure: trabecular, woven, plexiform, lamellar or Haversian. For lamellar bone, mechanics is known to play a crucial role in the orientation of the osteons and osteon morphotypes [13] that results in different proportions of osteons with longitudinal fibers adapted to regions under predominant tension and osteons with slanted fibers adapted to zones under predominant compression respectively [14]. Therefore osteocyte *in situ* mechanical microenvironment is difficult to precisely quantify due to the cell dentritic complex shape and the ECM (Extra Cellular Matrix) highly hierarchical structure. The dentritic cell morphology is characteristic of their full differentiation but is key to enable their mechano-sensitivity. It is essential to quantify the relationship between *in situ* mechanical stimulation and the cell biological response to design successful regenerative therapies.

As bone displays multiple levels of porosities where interstitial fluid can circulate in the vascular porosity, the canaliculi and even small spaces between hydroxyapatite (HAP) platelets and the collagen fibers [15], several in vitro investigations of osteocyte mechanobiology have been made on cultured cells that are subjected to direct physiological shear fluid flow [16–20] of about 0.8 to 3 Pa [21] in parallel plate flow chambers or cells reseeded on different substrates such as collagenous hydrogels mimicking osteid [22,23] or various biomaterials scaffolds [24–28] in 3D perfusion bioreactors to produce shear flow stimulation. In 3D bioreactors, cells in animal bone explants have also been directly studied [28–30]. Other systems studied the effect of pressure on cells seeded on trabecular bone [31]. Both fluid shear flow and mechanical stimulations of the cell substrate has also been tested [32].

Bone is also a mineralized solid tissue and another type of investigation of osteocyte mechanobiology has then focused on direct mechanical stimulations of the substrate in explants or man-made collagenous or mineralized matrices that where cells were reseeded. These investigations follow the concept of ”mechanostat” developed by Frost in 1987 [33,34]. In vivo [34,35] measurements showed bone resorption below 0.03% strain, usual physiological stimulations between 0.03% to 0.15% strain and bone mass increase between 0.15% to 0.3% strain through bone remodeling. The first in vitro systems mechanically stimulating the matrix used silicone membranes on which the cells were seeded but required strains to induce an osteogenic response around 1% to 10% that were higher than in bone and would produce cracks in bone [32,36]. It seemed important that the morphology of the systems is a key factor to reproduce in vitro strains on the cells in a manner that would be more similar to the strains the developed by the lacuna-canaliculi systems in vivo [37]. Systems that could generate mechanical stimulations (usually compression) closer to the physiological conditions on single cells [38] in a group or different cell parts (body and processes) [39], or in animal explants of bone fragment [40] or entire small animal bones [41] were then initiated.

For various application studies where human MSCs are reseeded, in vitro systems based using different natural or synthetic scaffolds such as nacre [42], coral [43], bioglass [44], polymers [45, 46], titanium [47], ceramics, Hap or demineralized bovine bone have been

employed for single or multiple cell types co-cultures. Osteocytes have also been shown to be sensitive in vitro to 13kPa hydrostatic pressure [48, 49, 50, 51] and 0.3-3 Pa shear stress [18] and direct contact pressure [39]. These systems have provided good in vitro models for human bone cells co-culture to study their mechanotransduction usually over a period that does not exceed 28 days. The limitations of these models include the absence of physiologically relevant scaffold coupled with mechanical stimuli and concurrent modeling with geometrical simplifications.

In contrast to shear flow or mechanical pressure stimulations of cells or cellularized bone explant, the mechanical stimuli in the presented bone-on-chip specifically addressed loading directly on human bone tissue (either cortical or trabecular bone) to stimulate human (or animal) cells attached to the tissue by integrins. The systems allowed micro physiological fluid flow within the tissue when the bone is mechanically loaded in chambers containing the cellularized bone immersed in the conditioned media. Previous study in the literature investigated the differentiation of mouse MSC into stem cell derived osteocytes on a mineralized medium that was mechanically loaded up to 28 days and using a differentiating media [71]. The presented study concerns human MSCs on human bone for over 26 months with the use of a differentiating media.

MATERIAL AND METHOD

Dual experiment and 3D multi-cellular multi-scale modeling investigates stem cell derived osteocyte mechanobiology in bone-on-chip composed of human MSCs differentiating into osteocytes reseeded on human bone.

Sample preparation and cell reorganization

The bone-on-chip are composed of one to five hundred micron thick samples harvested from fresh bone from cadaveric or surgical sources seeded with hMSC or mouse early osteocytes (MLOY4) to compare the cell reorganization at the progenitor and differentiated stage in the early days of seeding. The bone samples preparation follow a cutting protocol. The fresh human cortical or trabecular bones were decellularized using a protocol using multiple bathing steps with alcoholic Daquin solution, a detergent, a protease and antibiotics. The bones were reseeded with cells at a concentration 10^5cells/ml. In these recellularized bones the cells reorganized in vitro as they would in vivo in Figure.1: the MSC migrated into the Haversian canals as early as at 10 days and along the large flat surfaces of the bone samples [14], and the osteocytes (MLOY4) relocated on the mineralized ECM arranged in a network with a stabilized population over 26 months. Note that after 30 days in the systems initially cellularized with MScs, the Haversian canals and the flat surfaces were covered by cells resembling bone lining cells [7, 27] and osteocytes bearing long processes were observed at 547 days. The bone-on-chip were maintained alive for over 26 months using alpha MEM with 1x antibiotic and 10% bovine serum.

Experimental setting for osteocyte stimulation in newly formed bone versus native bone

The bone-on-chip were subjected to two types of mechanical stimulation. First the bone-on-chip underwent a regular low stimulation by free fall drop of medium above the bone formation region that produced a compressive pressure of few tens of kPa and a shear stress of about 10 Pa [52]. The frequency was of 1Hz for about 5 min every other day. This regime of mechanical

stimulation represented a resting situation for a human victim of a bone fracture in Figure 2B. Second the bone on chip were subject to a three point bending mechanical loading in a in a unique miniaturized customized machine under a Nikon-Eclipse TE 200-U (B2OA Lab at University Paris 7) fluorescence microscope with an optical resolution 1.42 µm $px^{-1}$for short time experiment of about 30 minutes in Figure 2A. These mechanical stimulations under fluorescent microscopy made it possible to measure the variation of the cytoplasmic calcium concentration in the cells while mechanically stimulated. This experimental setting was used to create an in vitro microenvironment closely mimicking bone in vivo environment and study the mechanical stimulation on mature osteocytes in native bone and on MSCs to stem cell derived osteocytes in newly formed bone-like tissue.

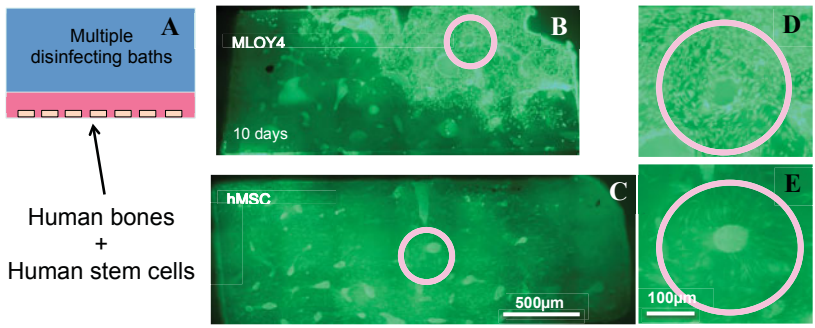

Figure 1. A: human bone samples undergoing a decellularization protocol, B: human cortical bone sample recellularized with MLOY4 at 10 days of culture, C: human cortical bone sample recellularized with human MSCs at 10 days of culture, D: Zoom of the MLOY4 cells reseeded and reorganized around an osteon shown in B, E: Zoom of the MSCs cells reseeded and reorganized around an osteon and inside an Haversian canal shown in C

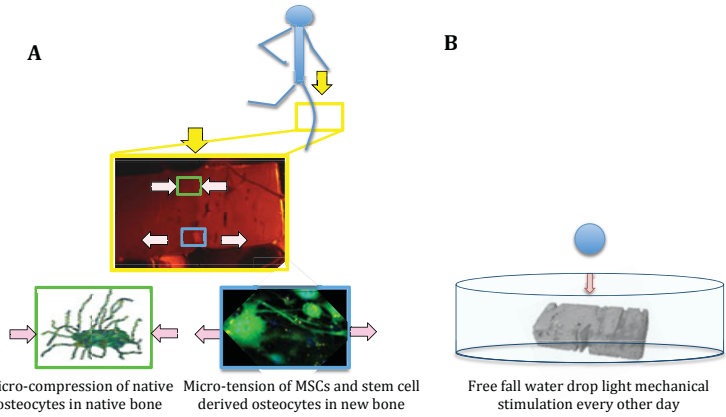

Figure 2. Mechanical stimulations: A: experimental three point bending test applied to the cellularized bone samples over a short period of time to study the osteocyte mechanobiology at different stages of their differentiation and to assess the mechanical microenvironment around mature osteocytes in native bone and around MSCs and stem cell derived osteocytes in newly formed bone-like tissue; B: low mechanical stimulations applied to the the bone-on-chip using free fall water drop every other days.

Hierarchical multiscale model of osteocyte 3D microenvironment

Concurrent in vitro experiments and in silico modeling of the mechanically stimulated bone-on-chip were implemented. The numerical model was hierarchical and included a tissue scale and a cell scale. The computational models were 3D image-based multi-scale finite element model (FEM). At the tissue scale, the real geometry was reconstruction from micro CT imaging (Skyscan 1176, Bruker at B2OA, Paris) with a 4 µm resolution [53]. The osteonal sub-structures were reconstructed using successive grey level segmentation in the transverse plan of the osteon axis and an interpolation along the osteon axis [54] in Figure 3. The generated meshes with a 10 µm resolution were exported into an FEM software [55]. The fresh bone mechanical properties and stress field were identified through a dual experimental and numerical method that followed a top-down approach in order to validate theoretical hypotheses on the multi-scale failure mechanisms [56, 57] in 2D and 3D. The local elastic Young's moduli were correlated to the phase mineral content that was correlated to the local grey scale averaged in each osteon [58, 59, 60, 61, 62, 63]. The elastic moduli were not segmented at individual pixel level [64, 65]. The range of the Young's moduli values were determined by nanoindentation data points using a Berkovitch tip [58, 66] at a constant strain rate ($5\ 10^{-2}\ s^{-1}$) in order to calibrate the grey scale. The nanoindentation measurements were performed in humid conditions using a commercial instrument (nanoindenter XP (MTS, Minneapolis, USA)) on the sample face showing the longitudinal and transverse direction of the osteons in order to measure the osteon transverse and longitudinal Young's moduli.

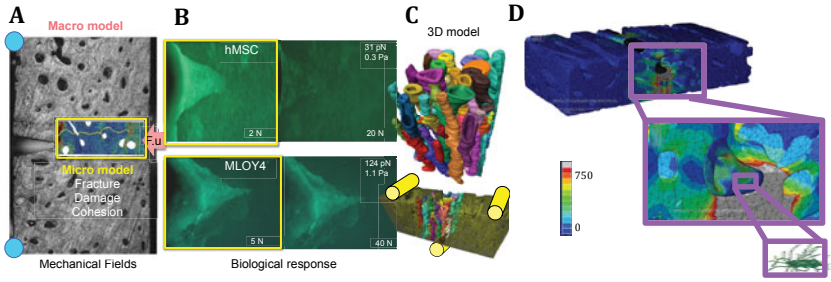

Figure 3. A: Three point bending experimental setting; B: Calcium concentration variation in MSCs and MLOY4 cells subjected to mechanical stimulations and measured under fluorescent microscopy; C: cortical bone tissue 3D osteon cluster reconstruction; D: Von Mises stress field (MPa) within an osteon that serve as boundary conditions for the cell scale model.

The elastic moduli distributions were determined from the indentation load-displacement curves using the method described by Oliver and Pharr [58] and adjusted using the method described in [66] to account for the osteon anisotropy [67]. The transverse and longitudinal Young's moduli of the osteons ranges from 9.125 and 15.25 GPa (E_{min}) that was associated with the grey level denoted as f_{min} to 17.62 and 23.34 GPa (E_{max}) that was associated with the grey level denoted as f_{max}. The local Young's modulus E_I of osteon I within a representative square domain Ω_I was calculated by averaging the grey levels f_g of the $n_{\Omega I}$ pixels as follows:

$$E_I = E_{min} + \frac{\left(\frac{1}{n_{\Omega_I}}\sum_{g\epsilon\Omega_I} f_g\right) - f_{min}}{f_{max} - f_{min}}(E_{max} - E_{min})$$

The Poisson's ratios were determined by microextensometry with a mean value of 0.23 and a standard deviation of 0.04 and were inversely correlated to the phase grey levels [56, 57]. The local Poisson ratio of osteon I was therefore calculated as follows:

$$\upsilon_I = \upsilon_{max} - \frac{f_{max} - \left(\frac{1}{n_{\Omega_I}}\sum_{g\epsilon\Omega_I} f_g\right)}{f_{max} - f_{min}}(\upsilon_{max} - \upsilon_{min})$$

The cement lines Young's moduli were taken 25% lower than their encapsulated osteons based on nanoindentation measurements observed in the literature and not their grey levels. Cement line Poisson's ratio were taken equal to 0.49 owing to their specific protein composition [56]. Each osteon was considered transverse isotropic and characterized by 5 elastic moduli: E_T, E_L, υ_T, υ_{TL}, G_{TL}. The shear modulus of osteon I is calculated as follows:

$$G_I = G_{min} + \frac{\left(\frac{1}{n_{\Omega_I}}\sum_{g\epsilon\Omega_I} f_g\right) - f_{min}}{f_{max} - f_{min}}(G_{max} - G_{min})$$

Based on the real bone morphology, the model validated theoretical hypotheses on bone mechanical constitutive law (heterogeneity, micro movement from sliding contact interfaces, damage [15]) by calculation of the energetic balance between the micro scale inside a region of interest (ROI) near the stress concentrators (micro damage) and the macro scale experimental

measurements [56]. The Young's moduli of the bone osteon heterogeneities were measured by nanoindentation. A frictional interface between the osteons and the interstitial bone represented the cement line. The multi-scale image-based FEM model was subjected to the same experimental boundary conditions and validated by the experiment. The bone-on-chip were mechanically loaded to remain in the elastic region of the tissue to minimize the damage inflected to the cells and as the purpose of the study was to investigate the bone formation phase after an controled micro fracture (i.e. the micro indent in the three point bending samples) and not the remodeling process. The resulting model quantified the local forces and micro damage sensed by live osteocytes and MSCs in situ and to be transmitted to the cell scale model [58].

At the cell scale the real geometry of a characteristic mature osteocyte was reconstructed from confocal images (Leica SP2 at LBPA Lab at ENS Cachan) with a resolution of 0.18 μm in the xy plane and 0.51 μm in the z-direction. This was a preliminary model to reconstruct the geometry of a cell and only one type was considered. The images were postprocessed in order to extract the cell body contours and the central axes of the cytoplasmic processes [69]. The volume structure of the cell body and processes were built by a 3D geometrical algorithm and then meshed [70]. The meshes of the cell constituents were then imported and assembled in an FEM solver [54]. The cell homogenized Young's modulus (cytoplasm and cytoskeleton) was taken as 4.47 kPa and a Poisson ratio of 0.4 and the cell nucleus Young's modulus of 17.88 kPa and a Poison ratio of 0.4 [71]. Osteocytes with their cytoplasmic processes and attached to their PCM (peri cellular matrix) by tied constraints to sense mechanical stimulations in the mineralized ECM were explicitly modeled from segmentation of confocal microscopy images. The pericellular matrix Young's modulus was chosen to be equal to 40 kPa and its Poisson ratio equal to 0.4 [72]. The bone ECM was either modeled as anisotropic with a Youngs modulius of 16 Gpa and a Poisson ratio of 0.3 or anisotropic with varying properties to represent either young or more mature bone. The cell model investigated either mature osteocyte in native bone under physiological compression in Figure 4 or MSCs or SCDO under micro tension in newly formed bone in Figure 5B.

DISCUSSION

Stem cell derived osteocytes morphological and secretome chracterization

In the first days following reseeding, hMSCs migrated to fill empty cavities such as the controled indent and the Haversian canals in Figure 1 and then secreted a fibrous matrix. A different behavior was observed with MLOY4 that migrated to reorganize on the native mineralized bone around osteons and secreting with a thinner matrix layer. Both of these newly formed matrices were shown to contain collagen type 1 and mineral crystals at 39 days [73]. After 109 days of culture, noticeable changes in the newly formed matrix structure were observed in the systems seeded with differentiating hMSCs. Within the matrix lamellae with alternating collagen undergoing mineralization appeared and the cells with a distribution similar to the one seen for osteocytes in osteons was showed. The cells reorganized *in vitro* as they would *in vivo* at the different stage of differentiation and produced a mineralizing collagen I fibrous ECM at 109 days of which the strength was a quarter of native bone and was more elasto-plastic in Figure 6A. Histochemistry of fixed samples showed calcium minerals and collagen type I at 39 days.

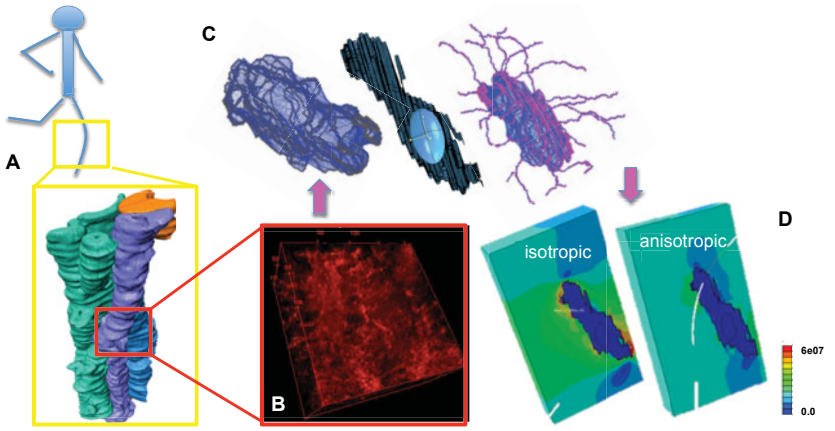

Figure 4. Osteocyte model: A: 3D reconstruction of three osteon cluster from micro CT imaging of cortical bone tissue harvested in a human tibia that is subjected to micro compression during walking; B: confocal microscopy imaging using red autofluorescence of a mature osteocyte in native human cortical bone; C: 3D reconstruction of a mature osteocyte from confocal microscopy observations; D: the resulting stress field (MPa) due to a physiological micro compression during walking around the cell when subjected to a physiological 2,000 micro strain compression when the mineralized ECM is considered either isotropic or anisotropic.

Morphological and secretome characterization of early and more mature stem cell derived osteocytes was performed under confocal microscopy (i.e. Leica SP8 at LBPA Lab at ENS Cachan) with x10, x40, x60 and x100. The presence of bone lining cells like was also noticed near the external edges of the new bone in the indent and along the external edges of the native bone and the substructure display resemblance to the inner circumferential lamella. Some cells within the newly formed tissue in the crack indent were organized in a network and connected by long processes in Figure 5B. In situ immunochemistry revealed the production of E11 and sclerostin by early and mature stem cell derives osteocytes at 640 days in Figure 6B.

Bone stromal cell mechanibiology

Osteocytes detect stress in vivo from fluid flow through primary cilia and glycolalyx, sense other cells and attached to them through connexins [74] and detect stress in the bone matrix through either trans-membrane integrin anchor proteins or pericellular matrix (PCM) filament attachments between the cell actin/fibrin filaments and either canaliculi projections or cell body wall [31, 54, 59]. Osteocytes respond to mechanical stimulations by reorganizing their cytoskeletons [75, 76], releasing ions and chemicals through their membrane channels [39, 77] and modulating the proteins and minerals they secrete [30]. Previous studies identified many mechanotransduction pathways [78, 79, 80, 81]. When derived from mesenchymal stem cells in vitro the progressing gene expression of the cell differentiation into osteocytes can be tracked over multiple days usually up to 28 days [82]. Close cooperation between mature osteocytes and their progenitors exists to detect defects and initiate remodeling [2, 83]. Intra canalicular flow ensure communications between osteocytes and osteoblasts [84, 85]. In the presented bone-on-

chip a mixed cell populations was generated. The *in situ* calcium response of the cells at different differentiation stages to *in situ* mechanical loads were measured *in vitro* by the released calcium concentration variations under mechanical load in confocal microscopy as shown in Figure 6C.

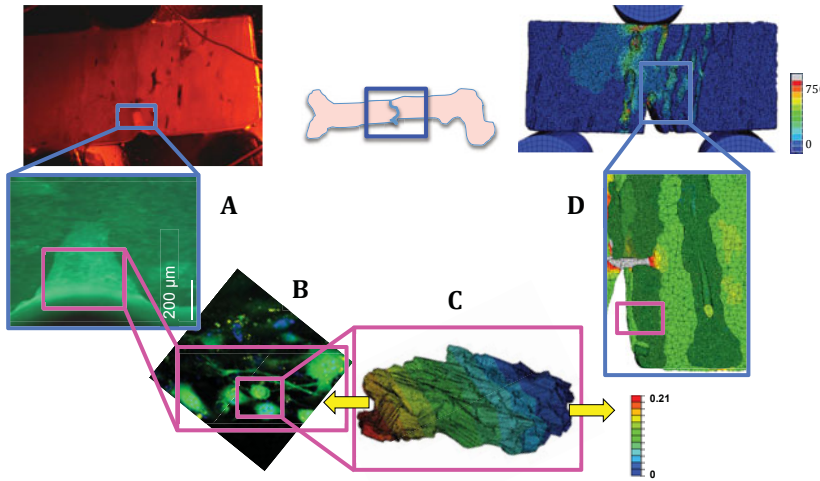

Figure 5. MSCs and stem cell derived osteocytes under micro tension in the newly formed bone-like matrix: A: cytoplasmic calcium concentration variation in MLOY4 cells inside the newly formed bone-like matrix; B: confocal imaging of SCDOs at 19 months; C: displacement field (µm) in the body of SCDOs under 100 pN local micro tension; D: Von Mises stress field (tissue scale (top)) inside a cortical bone sample and tensile stress field inside an osteon located in the vicinity of a crack indent (picture underneath) that defines the region of interest (ROI) of which the boundary are the edges of the cell scale model.

The mechanical stimulations were in the range of 1500 to 2000 µε to mimmick mechanical loads that would cyclically occur during walking in a human for nearly 30 minutes. No excessive load was applied that could lead to a de-differentiation [86]. The results are in agreement with the finding from other research using fluid flow stimulation.

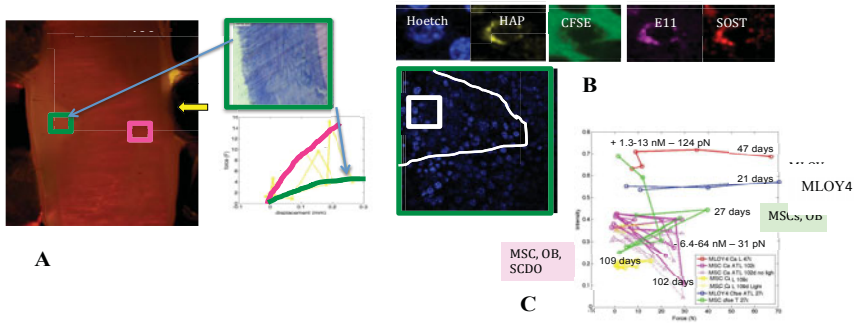

Figure 6. Secretome: A: newly formed bone-like matrix and its collagen lamellar structure with alternate orientations and the load-deflection response of native bone in red and the bone-like matrix in green; B: in situ histochemistry characterization of stem cell derive osteocytes secretome that displays HAP, E11 and sclerostin in varying amount in the bone formation region; C: MSCs and osteocytes in situ cytoplasmic calcium response as a function of the micro mechanical stimulation applied to the cortical bone sample in a three-point bending test.

CONCLUSION

All the cells were mechanically stimulated by the application of micro-load to the bones where the cells reside in custom-made and customized testing machines. The bone-on-chip mimicked in vitro an environment that was close to the in vivo and was representative of native bone environment. The bone-on-chip investigated the bone formation phase in a more that a previous crack indent and quantified the stress on the cells due to micro-tension. The bone-on-chip also investigate the compressive stress on a cell having the morphology of a mature osteocyte in the native bone. The mechanical stimulations on the cells in the native tissue were compared to within the newly formed bone. The live systems were ponctually imaged under confocal microscopy to concurrently measure the calcium variation under controled mechanical load and to characterize the cell morphological changes during the MSC diffrentiation into stem cell derived osteocytes without the addition of diffrentiating media and when subjected to low intensity regular mechanical stimulation. Cleaned and decellularized human bone represented a physiologically relevant scaffold for in vitro co-cultures MSCs to create SCDO and therefore ensuring the tissue functionnalization and osteogenicity. The systems made it possible for continuous tracking of the human cells secreted mineralizing fibers to create lamellae in situ.

ACKNOWLEDGMENT

The authors are grateful to the finanacial support from NSF CMMI BMMB 1214816 EAGER award, the Farman Institute for OLA, Bone Labs, and Bonoclisflum projects and the CNRS GC94 grant. The authors are also grateful for help to keep the bone-one-chips alive from Nathanael Larochette and Marianne Bourguignon. The authors are also grateful to Hanane El

Farci for her ingenuity with the histology methods. The authors are grateful to Dr. Boumedjem Rakka for his comments on the boundary conditions at the tissue scale. The authors thanks undregraduate students Willy Haik, Romeo Antier, Thibault Marsan, Florian Mainnemare, Guillaume Lostec et Johan Dhuimieres for their help with the osteocyte confocal image post-treatment.

REFERENCES

1. D.R. Carter, W.C. Hayes, and D.J. Schurman. J. Biomech. **9**, 211–218 (1976).
2. D.R. Carter and W.C. Hayes, J. Biomech., **10**, 325–337 (1977).
3. Y.N. Yeni and D.P. Fyhrie, Bone, **30**(3), 509–514 (2002).
4. E. Budyn, M. Bensidhoum, T. Marsan, F. Mainnemare, P. Tauc, S. Sasnouski, E. Schmidt, E. Deprez, H. Petite, Proc. CMBE 2015, **1**, 124-127, (2015). ISBN 978-0-9562914-3-1
5. D. Taylor, J.G. Hazenberg, and T.C. Lee, J. Biomech., **36**, 121–124 (2003).
6. L.F. Bonewald, M. Johnson, and M. Kneissel. Bone, **54**, 181, (2013).
7. S.C. Miller, Calcified Tissue Internat., **41**, 1–5, (1987).
8. S.Y. Boateng, T.J. Hartman, N. Ahluwalia, H. Vidula, T.A. Desai, and B. Russell, Osteoporos. Int,, **25**(Supp 3), S487– S489, (2014).
9. D.N. Menton, D.J. Simmons, S.L. Chang, and B.Y. Orr, Anatom. Rec., **209**, 29–39, (1984).
10. L.S. Bella, M. Kayser and C. Jones. Am. J. Phys. Anthropol., **137**, 449456, (2008).
11. Y. Wang, L.M. McNamara, M.B. Schaffler, and S. Weinbaum. PNAS, **104**(40), 1594115946, (2007).
12. L.M. McNamara, R.J. Majeska, S. Weinbaum V. Friedrich, and M.B. Schaffler. Anat. Rec., **292**, 355–363, (2009).
13. J.G. Skedros, K. Keenan, D.M.L. Cooper, and R.D. Bloebaum. J. Struct. Biol., **187**, 129–148, (2014).
14. J.G. Skedros, K Keenan, T.J. Williams, and C.J. Kiser, J. Struct. Biol., **181**, 95–107, (2013).
15. S.C. Cowin and L. Cardoso.. J. Biomech., **48**, 842–854, (2015).
16. M. Mullender, A.J. El Haj, Y. Yang, M.A. van Duin, E.H. Burger, and I.J. Klein-Nulend. Medical and Biol. Eng. Comput., **42**, 14–21, (2004).
17. J.C. McGarry, I.J. Klein-Nulend, and P.J. Prendergast. Biochem. Biophys. Res. Com., **330**, 341348, (2005).
18. J. Klein-Nulend, R.F. M van Oers, A.D. Bakker, R.G. Bacabac, A. Vatsa, and S. Weinbaum.. Bone, **54**, 182–190, (2013).
19. Y. Wang, L.M. McNamara, M.B. Schaffler, and S. Weinbaum.. J. Musculoskelet, Neuronal Interact, **8**(4), 332– 334, (2008).
20. X. Sun, E. McLamore, V. Kishore, M. Slipchenko, D.M. Porterfield, and O. Akkus, Bone, **50**, 581–591, (2012).
21. S. Weinbaum, S.C. Cowin, and Y. Zeng. J. Biomech., **27**(3), 339–, (1994).
22. J. Parreno, G. Herd-Buckley, I. De-Hemptinne, and D.A. Hart, Mol. Cell. Biochem, **317**, 21–22, (2008).
23. M. Pridaux, A.R. Wijenayaka, D.D. Kumarasinghe, R.T. Ormsby, A. Evdokiou, and D.M. Findlay. Calcif. Tissue Int., **95**, 183–193, (2014).
24. D.W. Hutmacher, Biomaterials, **21**, 25292543, (2000).
25. B. Stevens, Y. Yang, A. Mohandas, B. Stucker, and K.T. Nguyen. J. Biomed. Mater. Res. B, **85**B, 573582, (2008).
26. S. Bose, M. Roy, and A. Bandyopadhay. Trends Biotechnol., **30**, 546554, (2012).
27. E. Budyn, M. Bensidhoum, T. Marsan, F. Mainnemare, P. Tauc, E. Deprez and H. Petite, Proc. ECCOMAS Coupled Problems, **1**:1-10, (2015).
28. S.M. Woo, J. Rosser, V. Dusevich, I. Kalajzic, and L.F. Bonewald. JBMR, **26**(11), 2634–46, (2011).
29. E.H. Davidson, D.D. Reformat, A.A. Orlando Canizares, P.B. Saadeh I.J. Wagner, and S.M. Warren. J. Tisssue Eng. Regen. Med., **6**, 769–776, (2012).
30. S. Marino, K..A Staines, G Brown, R.A. Howard-Jones, and M. Adamczyk. BoneKEy Reports, **5**(818), 1–18, (2016).
31. E. Takai, R.L. Mauck, C.T. Hung, and X.E. Guo. J. Bone Min. Res., **19**(9), 1403–10, (2011).
32. J. You, C.E. Yellowhey, H.J. Donahue, Y. Zhang, Q. Chen, and C.R. Jacobs.. ASME J. Biomech. Eng, **122**, 387–, (2000).

33. H.M. Frost, Anat. Rec., **219**, 1–95, (1987).
34. H.M. Frost. Anat. Rec. A Discov. Mol. Cell. Evol. Biol., **275**, 10811101, (2003).
35. R. Al Nazer, J. Lanovaz, C. Kawalilak, J.D. Johnston, and S. Kontulainen. J. Biomech., **45**, 27–40, (2012).
36. J. Klein-Nulend, A. Van Der Plas, C.M. Semeins, N.E. Ajubi, J.A. Frangos, P.J. Nijweide, and E.H. Burger. Res. Com., **9**, 441–445, (1995).
37. A.R. Bonivtch, L.F. Bonewald, and D.P. Nicolella. J. Biomech, **40**, 21992206, (2007).
38. T. Adachi, Y. Aonuma, M. Hojo, M. Hojo, and H. Kamioka. Biochem. Biophys. Res. Comm., **389**, 495500, (2009).
39. T. Adachi, Y. Aonuma, M. Hojo, T. Takano-Yamamoto, and H. Kamioka. J. Biomech., **42**, 19891995, (2009).
40. T. Adachi, Y. Aonuma, S.-I. Ito, M. Tanaka, M. Hojo, T. Takano-Yamamoto, and H. Kamioka. J. Biomech., **42**, 2507–2512, (2009).
41. D. Jing, A. D. Baik, X. L. Lu, B. Zhou, X. Lai, L. Wang, E. Luo, and X. E. Guo. The FASEB J. Res. Comm., **28**, 1582– 1592, (2014).
42. E. Lopez, B. Vidal, S. Berland, S. Camprasse, G. Camprasse, and C. Silves. Tissue and Cell, **24**(5), 667–679, (1992).
43. J.M. Sautier, J.R. Nefussi, H. Boulekbache, and N. Forest, Soc. for in vitro biol., **26**(11):1079–1085, (1999).
44. I.D. Xynos, M.V. J Hukkanen, J.J. Batten, L.D. Buttery, L.L. Hench, and J.M. Polak. Calcif. Tissue Internat., **67**, 312–329, (2000).
45. S.L. Ishaug, G.M. Crane, M.J. Miller, A.W. Yasko, M.J. Yaszemski, and A.G. Mikos. Journal of Biomechanical Materials Research, **36**, 1728-, (1997).
46. J.T. Schantz, D.W. Hutmacher, K.W. Ng, H.L. Khor, T.C. Lim, and S.H. Teoh. The International Journal of Oral and Maxillofacial Implants, **17**(2), 161–174, (2002).
47. G.N. Bancroft, V.I. Sikavitsas, J. van den Dolder, T.L. Sheffield, C.G. Ambrose, J.A. Jansen, and A.G. Miko.. PNAS, **99**(20), 12600–12605, 2002.
48. J. Klein-Nulend, A. Van Der Plas, C. M. Semeins, N. E. Ajubi, J.A. Francos, P.J. Nijweide, and E. H. Burger. The FASEB Journal, **9**(5), 441-445, (1995).
49. S. Scheiner, P. Pivonka, and C. Hellmich. Biomech. Model. Mechanobiology, **9**, 9-28, (2016).
50. C. Morin, and C. Hellmich. Ultrasonics, 54, 1251-1269, (2014).
51. C. Hellmich, D. Celundova, and J. Ulm. Journal of Engineering Mechanics, **135**(5), 382-394, (2009).
52. A. Nouhou Bako, F. Darboux, F. James, C. Josserand and C. Lucas. Processes and Landforms, **41** (9), 199-1210, (2016).
53. SKYSCAN NV. NRecon User Manual. (2011).
54. FEI. Avizo 8: Avizo User's Guide. (2014).
55. Dassault Syst`emes. Abaqus 6.12: Abaqus/CAE User's Manual. (2012).
56. J. Jonvaux, T. Hoc, and E. Budyn, International Journal of Numerical Methods in Biomedical Engineering, **28**(9), 974–998, (2012).
57. P. Hasslinger, V. Vass, A. Dejaco, R. Blanchard, G. Örlygsson, P. Gargiulo, and C. Hellmich. International Journal for Numerical Methods in Engineering Science and Mechanics, **17**(3), 222-244, (2016).
58. S. Sanders, M. Bensidhoum, and E. Budyn, ZetaComputational Resources Ltd , Proc. CMBE 2015, **1**:132–135, (2015). ISBN: 978-0-9562914-3
59. W. Oliver and G.M. Pharr. Journal of Materials Research, **7**(6), 1564–1583, (1992).
60. E. Budyn, M. Bensidhoum, T. Marsan, F. Mainnemare, S. Sasnouski, P. Tauc, E. Deprez, and H. Perite. Coupled Problems in Science and Engineering VI, 6th International Conference on Computational Methods for Coupled Problems in Science and Engineering (Coupled Problems), **1**, 566-575, (2015).
61. E. Budyn, J. Jonvaux, and T. Hoc. International Journal for Numerical Methods in Biomedical Engineering, **28**(8), 815-837, (2012).
62. E. Budyn, J. Jonvaux, and T. Hoc. Journal of Applied Mechanics – Transaction of the ASME, **79**(2), 021001, (2012).
63. E. Budyn, and T. Hoc. Proceedings of the ASME 11th Biennal Conference on Engineering Systems design and Analysis, vol. **4**, 271-278, (2012).
64. E. Budyn, J. Jonvaux, C. Funfschilling, and T. Hoc. Journal of Applied Mechanics – Transaction of the ASME, **79**(1), 011008, (2012).
65. R. Blanchard, A. Dejaco, E. Bongaers, and C. Hellmich. Journal of Biomechanics, **46**, 2710-2721, (2013).
66. G.A.P. Renders, L. Mulder, L.J. van Ruijven, G.E.J. Langenbach, and M.G.J. van Eijden, Journal of

Biomechanics, **44**, 402-407, (2011).
67. J.G. Swadener, J.Y. Rho and G.M. Pharr. Journal of Biomedical Materials Research, **57**, 108–112, (2001).
68. L. Salguero, F. Saadat, and I. Savostianov. Journal of Biomechanics, **47**, 3279-3287, (2014).
69. C.A. Schneider, W.S. Rasband and K.W. Eliceiri , *Nat. Methods*. **9** (7), 671–675. (2012).
70. C. Geuzaine and J.F. Remacle, Int. J. Num. Meth. Eng., **79**(11), 1309–1331, (2009).
71. T.J. Vaughan, C.A. Mullen, SW. Verbruggen and L.M. McNamara, Biomech Model Mechanobiol., **14**, 703–718 (2016).
72. P. Varga, B Hesse, M. Langer, S Schrof, N.M. annicke, H. Suhonen, A. Pacureanu, D. Pahr F. Peyrin, and K. Raum. Biomech Model Mechanobiol, **14**, 267–282, (2015).
73. E. Budyn, M. Bensidhoum, S. Sanders, E. Schmidt, P. Tauc, E. Deprez and H. Petite. European Cell and Materials Conferences, **32**(supp. 4), 32, (2016).
74. C. Wittkowske, G.C. Reilly, D. Lacroix, and C.M. Perrault. Frontiers in Bioengineering and Biotechnology, **4**:1–22, (2016).
75. R.L. Duncan and C.H. Turner. Calcif. Tissue Int., **57**, 344–58, (1995).
76. J. Klein-Nulend, R.G. Bacabac, and A.D. Bakker. Eur. Cell. Mater., **24**, 278–291, (2012).
77. L. F Bonewald. Journal of Bone and Mineral Research,, **26**(2), 229–238, (2013).
78. L.F. Bonewald and M.L. Johnson, Bone, **42**(4), 606 – 615, (2008).
79. M. Pridaux, D.M. Findlay, and G.J. Atkins.. Curr. Opin. Pharmacol., **28**, 24–30, (2016).
80. A. Nather, V. David, J.W. .H. Teng, C.W. Lee, and B.P. Pereira, Annals Academy of Medicine, **39**(8), 599–606, (2010).
81. C.M. Runyan, A.T. Vu, A. Rumburg, K. Bove, J. Racadio, D.A. Billmire, and J.A. Taylor Plastic and reconstructive surgery, **136**(4), 461–473, (2015).
82. W.R. Thompson, G. Uzer, K.E. Brobst, Z. Xie, B. Sen**,** S.S. Yen, M. Styner and J. Rubin**,** Sci. Report, **5**, 11049, (2015).
83. J. Klein-Nulend, A.D. Bakker, and R.G. Bacabac, Osteoporosis Int., **25**, 1427-1437, (2014).
84. M.I. Pastrama, S. Scheiner, P. Pivonka, and C. Hellmich. Bone, **107**, 208-221, (2018).
85. G.H. Goldsztein. SIAM Journal of Applied Mathematics, **65**(6), 2128-2140, (2005).
86. D.B. Jones, H. Nolte, J.G. Scholübbers, E. Turner, and D. Veltel. Biomaterials, **12**, 101-110, (1991).